Structure optimization of high indium content InGaAs/InP heterostructure for the growth of $In_{0.82}Ga_{0.18}As$ buffer layer*

WEI Qiu-lin (魏秋林)[1], **GUO Zuo-xing** (郭作兴)[1], **ZHAO Lei** (赵磊)[1], **ZHAO Liang** (赵亮)[1], **YUAN De-zeng** (袁德增)[1], **MIAO Guo-qing** (缪国庆)[2], **and XIA Mao-sheng** (夏茂盛)[1]**

1. Key Laboratory of Automobile Materials of Ministry of Education of China, College of Materials Science and Engineering, Jilin University, Changchun 130025, China

2. State Key Laboratory of Luminescence and Applications, Changchun Institute of Optics, Fine Mechanics and Physics, Chinese Academy of Sciences, Changchun 130033, China

(Received 5 September 2016)

Microstructure and misfit dislocation behavior in $In_xGa_{1-x}As$/InP heteroepitaxial materials grown by low pressure metal organic chemical vapor deposition (LP-MOCVD) were analyzed by high resolution transmission electron microscopy (HRTEM), scanning electron microscopy (SEM), atomic force microscopy (AFM), Raman spectroscopy and Hall effect measurements. To optimize the structure of $In_{0.82}Ga_{0.18}As$/InP heterostructure, the $In_xGa_{1-x}As$ buffer layer was grown. The residual strain of the $In_{0.82}Ga_{0.18}As$ epitaxial layer was calculated. Further, the periodic growth pattern of the misfit dislocation at the interface was discovered and verified. Then the effects of misfit dislocation on the surface morphology and microstructure of the material were studied. It is found that the misfit dislocation of high indium (In) content $In_{0.82}Ga_{0.82}As$ epitaxial layer has significant influence on the carrier concentration.

Document code: A **Article ID:** 1673-1905(2016)06-0441-5

DOI 10.1007/s11801-016-6190-3

Due to the unique properties, ternary III-V compound semiconductor attracts more and more attention in recent years[1], which has been widely used in microelectronic and optoelectronic fields[2-4]. $In_xGa_{1-x}As$ ($0<x<1$), with features of relatively high carrier mobility, wide direct band gap ranging from 0.35 eV to 1.42 eV, high reliability and radiation resistance, has wide applications in short-wave infrared (SWIR) region. Particularly, high indium (In) content $In_xGa_{1-x}As$ (x=0.82) detectors with the cut-off wavelength of 2.5 μm[5,6] applied in aerospace imaging (such as earth observation, remote sensing and environmental monitoring) and spectroscopy attract more interests. To obtain high quality $In_{0.82}Ga_{0.18}As$/InP (100) structures, the lattice defect formation owing to misfit is the chief problem. Large lattice mismatch of about 2% existing in $In_{0.82}Ga_{0.18}As$/InP (100) heterostructure brings about amounts of stress in epilayer. The process of stress relaxation of the heterostructure is usually determined by the formation of dislocations which can further degrade the performance of the detectors[4,7]. The key point is the reduction of threading dislocations in InGaAs due to the relatively high lattice mismatch with respect to InP.

In this paper, to release the strain, the $In_xGa_{1-x}As$ layers are commonly employed as buffer for InP-based InGaAs. The threading dislocation density can be reduced for further epilayer growth. Through a comprehensive comparison, the effects of $In_xGa_{1-x}As$ buffer layer on the material quality, defect behavior and performance of $In_{0.82}Ga_{0.18}As$/InP (100) heterostructure are investigated. Based on transmission electron microscopy (TEM) images of the three typical structures, the misfit dislocation formation mechanism is also investigated.

$In_xGa_{1-x}As$/InP (100) heterostructures were grown by low pressure metal organic chemical vapor deposition (LP-MOCVD). The growth was performed using trimethylindium (TMIn), trimethylgallium (TMGa), and 10% arsine (AsH_3) in H_2 as precursors. Palladium-diffused hydrogen was used as carrier gas. The substrates on a graphite susceptor were heated by inductive coupling radio frequency power, the temperature was detected by a thermocouple, the reactor pressure was kept at 1×10^4 Pa, and the growth temperature was 450 °C.

* This work has been supported by the National Key Basic Research Program of China (No.2012CB619200), the National Natural Science Foundation of China (No.61474053), the State Key Laboratory for Mechanical Behavior of Materials of Xi'an Jiaotong University (No.20161806), and the Natural Science Basic Research Open Foundation of the Key Lab of Automobile Materials, Ministry of Education, Jilin University (No.1018320144001).

** E-mail: xiams@jlu.edu.cn

$In_xGa_{1-x}As$ layers with different In components x of 0.53 and 0.82 were deposited and marked with samples A and B, respectively. Then under the same conditions, sample C with $In_{0.82}Ga_{0.18}As$ buffer layer was prepared.

Transmission electron microscopy (TEM, JEM-2100F, JEOL) and high resolution transmission electron microscopy (HRTEM) were used for the detection of plane and [110] cross-section sample operating at 200 kV. The surface morphology of the samples was detected by atomic force microscopy (AFM, Multimode 8) and scanning electron microscopy (SEM, EVO-18). Raman scattering spectroscopy (UV-Horiba) and Hall tester (Lake-7704A) were used to measure the stress and Hall effect of the samples.

The surface morphologies of the $In_xGa_{1-x}As$ epitaxial layers got from samples A, B and C are shown in Fig.1. The uniform smooth surface with few defects can be seen in sample A. The corresponding surface height can be calculated from three-dimensional images of AFM to be approximately 30.0 nm. It is evident that the surface morphology of the sample B is relatively rough with many deep holes (in Fig.1(b)). From the corresponding AFM image, it can be found that large numbers of island-like shapes appear on the sample B surface, and the surface height difference is 316.0 nm. Fig.1(c) shows the morphology of sample C. Compared with sample B, the hole shapes decrease, and by using the $In_{0.82}Ga_{0.18}As$ buffer layer, the surface morphology is optimized obviously. The corresponding surface height is approximately 300.0 nm. It is noted that within the holes in the surface of samples B and C, some square holes marked with white arrow can be seen. In Fig.1(d), the holes show obvious square shapes and some plane information. The shape and orientation of the hole are very similar to those obtained on (100) InP with a concentrated HBr solution and in-situ etching of GaAs[8,9]. According to the growth orientation, the vectors of the hole have been marked. Another hole shape can be seen in Fig.1(e). Similar shape and orientation of these holes were obtained with in-situ etching of GaAs by molten KOH[10,11]. These holes like etch pits are seeded by dislocations in the substrate or the etched epitaxial layer.

In the case of lattice mismatch between the $In_{0.82}Ga_{0.18}As$ epitaxial layers and the InP substrate, mismatch stress in the epitaxial layer is very important for surface morphology, microstructure and properties of the sample. Based on the study of Raman scattering of $In_xGa_{1-x}As$ materials, due to the limitation of the scattering selection rule, the $In_{0.82}Ga_{0.18}As$ epitaxial layer of sphalerite structure will present different phonon modes under different back-scattering geometries[12,13]. There is only the TO mode under the (011) back-scattering and only the LO mode under the (100) back scattering, but the two modes will appear in the (111) back scattering[14]. The InAs-like LO frequencies almost remain near 233 cm^{-1} in $In_xGa_{1-x}As$ Raman scattering, while the GaAs-like LO frequency varies with the In content[15].

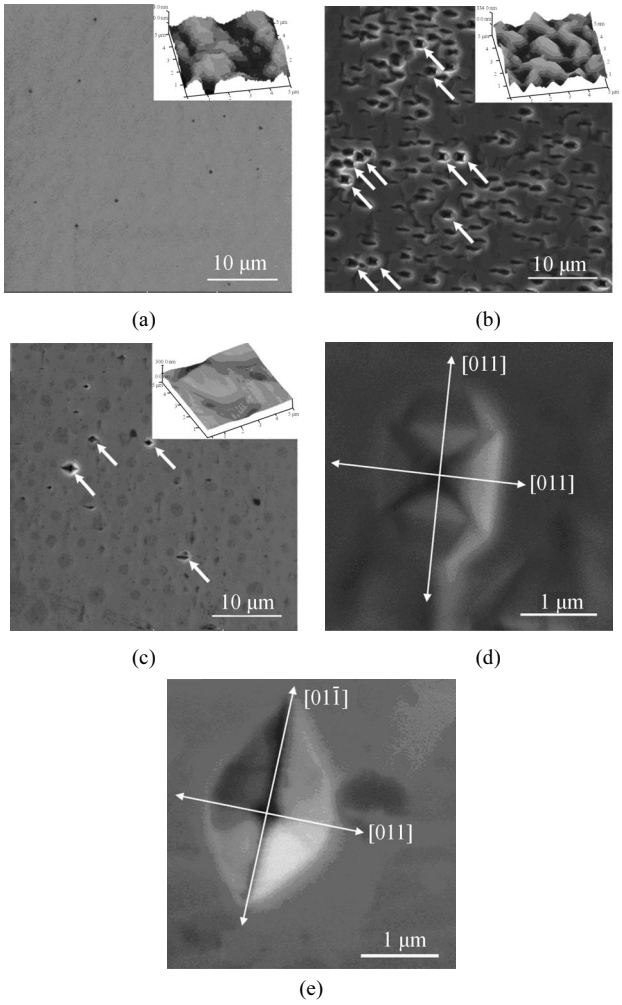

Fig.1 Surface morphologies of $In_xGa_{1-x}As$ epitaxial layers got from samples A, B, C with different growth parameters: (a) $In_xGa_{1-x}As$/InP (x=0.53); (b) $In_xGa_{1-x}As$/InP (x=0.82); (c) $In_xGa_{1-x}As$/InP with $In_xGa_{1-x}As$ buffer (x=0.82); (d) The magnified image of hole in (b); (e) The magnified image of hole in (c)

Fig.2 shows the (001) back-scattering Raman spectra of epitaxial layers of different samples. Tensile stress will make GaAs-like LO frequency move to the low frequency direction, while it moves to the direction of high frequency by compressive stress. As for InAs LO mode, the peak has not frequency shift when the compressive stress acts on epitaxial layer, but tensile stress will make its frequency move to the high frequency direction[15,16]. From Fig.2, it can be clearly seen that compared with the matched structure of sample A, the GaAs-like LO frequency of sample B moves to the high frequency direction, while the InAs-like LO frequency of sample B shows no frequency shift. But the GaAs-like LO frequency and InAs-like LO frequency of sample C both move to the high frequency direction.

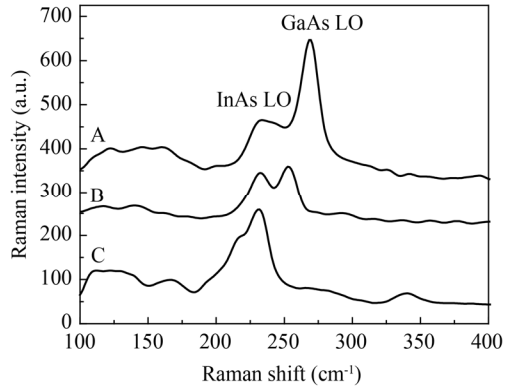

Fig.2 Raman spectra of the InGaAs epitaxial layers for samples A, B and C

The relationship between the frequency shift of GaAs-like LO of $In_xGa_{1-x}As$ film and stress in epitaxial layer is[17]:

$$F = \frac{3\Delta\Omega_{LO}}{\omega_0} / [(S_{11}+2S_{12})\frac{p+2q}{\omega_0^2} - (S_{11}-S_{12})\frac{(p-q)}{\omega_0^2}], \quad (1)$$

$$\Delta\Omega_{LO} = \Omega^{LO} - \omega_0^{LO}, \quad (2)$$

$$\omega_0^{LO} = -32.4x^2 - 18.6x + 290, \quad (3)$$

where $\omega_0{}^{LO}$ is the frequency of $In_xGa_{1-x}As$ epitaxial material in stress-free condition, Ω^{LO} is the measured value of GaAs-like LO frequency, ω_0 is the optical phonon frequency at k=0, p and q are the optical phonon deformation constants, S_{11} and S_{12} are the elastic constants, and x is In constant[18,19].

From Tab.1, it can be seen that the frequency shift $\Delta\Omega^{LO}$ of sample C is larger than that of samples A and B, and the stresses F of the samples A, B and C calculated using Eq.(1) follow $F_C > F_B > F_A > 0$. The phenomenon of mismatch stress generated in the sample A is owing to extension and movement of the micro defects in InP substrate, and the stress and strain in the epitaxial layer. For samples A and B, the residual strain in epitaxial layers increases with the increase of In content. For sample C, although the strain induced by lattice mismatch is mainly relaxed in the buffer layer, the high In content buffer layers produce more dislocations, which might be transmitted to the epitaxial layers, then the epitaxial layer of sample C exhibits a bigger residual strain.

To study the effect of lattice mismatch on the microstructure of $In_xGa_{1-x}As$ epitaxial layer, the TEM has been detected. Fig.3 is the cross-sectional TEM images of the samples A, B and C. It can be seen from Fig.3(a) and (b) that the dislocation density in epitaxial layer of sample B is greater than that in sample A. There are a lot of mismatch dislocations and threading dislocations at the interface of sample B, and the dislocations in epitaxial layer show nonuniform distribution. The dislocations in the epitaxial layer and at the surface mainly come from the extension of misfit dislocations at the interface, caused by the crystal lattice stress generated during the process of growth. In Fig.3(b), some kinds of dislocations can be seen: Form 1 marked as "1" presents the dislocation generated near the surface and extended to the surface; Form 2 marked as "2" presents the extended dislocations from the interface but not extended to the surface; Form 3 marked as "3" presents the new dislocation coming from the action between the extended misfit dislocations with the dislocation generated by the mismatch stress release; Form 4 marked as "4" presents the dislocations produced in the interface and disappearing near the interface. Therefore, the square shapes like etch pits seen in Fig.1(b) are mainly Form 1 and Form 2. Fig.2(c) shows the structure of sample C. It is obvious that the dislocation density of the epitaxial layer decreases and the surface tends to be smoother than that of sample B. The $In_{0.82}Ga_{0.18}As$ buffer layer effectively inhibits the extension of misfit dislocations at the interface and the generation of dislocations in the epitaxial layer.

Tab.1 In content x, mismatch (%), Ω^{LO} and $\omega_0{}^{LO}$, frequency shift $\Delta\Omega^{LO}$, stress F for different samples

Sample	In content x	Mismatch (%)	Epitaxial layer thickness (nm)	Ω^{LO} (cm^{-1})	$\omega_0{}^{LO}$ (cm^{-1})	$\Delta\Omega^{LO}$ (cm^{-1})	F (GPa)
A	0.53	0	1 000	271.37	271.04	0.34	0.16
B	0.82	2	1 000	254.90	252.96	1.94	0.91
C	0.82	-	3 000	255.42	252.96	2.46	1.16

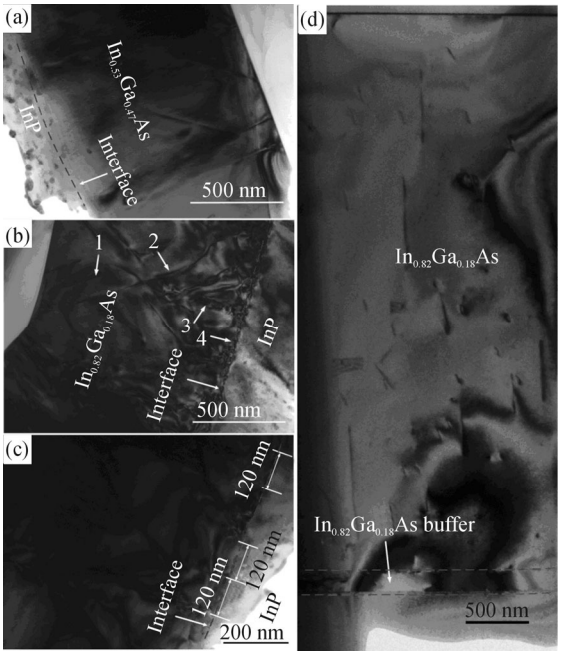

Fig.3 Cross-sectional TEM images of the InGaAs/InP: (a) Sample A; (b) Sample B; (c) Sample C; (d) Dislocation growth at the interface of sample B

In addition, certain regularity in the generation of the misfit dislocations at the interface has been found in the completely mismatch heterogeneous structure. The misfit dislocations regularity is more common in $In_xGa_{1-x}As$/GaAs heterogeneous structure and has been reported[20, 21]. But the phenomenon in this paper is rarely reported. As shown in Fig.4(a), a typical region is selected to be enlarged for observation. Misfit dislocations form at the equidistant positions, exhibiting period arrangement (shown as the white arrows 5, 6, 7). In one period, when the last atom of substrate corresponds to the last atom of the epitaxial layer, due to the effect of compressive stress, the atoms will be assembled at the interface, so the dislocations are generated at the equidistant positions. The lattice constants of InP substrate and the $In_{0.82}Ga_{0.18}As$ epitaxial layer are a_1=0.586 80 nm and a_2=0.598 54 nm, respectively[22]. An assumption has been made under the ideal condition: the (N+1)th substrate lattice and the Nth epitaxial layer lattice have the same distance h, as shown in Fig.4(c). The rule of the periodic arrangement of dislocations at the interface will be given as follows:

$$h=\frac{a_2}{a_2-a_1}\times a_1\approx 30\ \text{nm},\ N=\frac{h}{a_2}\approx 50\ . \tag{4}$$

The calculation error with the actual situation is

$$\frac{Na_2-(N+1)a_1}{a_2}\approx 0.03\%\ . \tag{5}$$

The calculated result shows that the minimum period is 30 nm, which consists of 50 $In_{0.82}Ga_{0.18}As$ epitaxial layer lattices and 51 substrate lattices. With the increase of the period distance, the error becomes larger, which makes the growth cycle length of dislocation be multiples of h. Fig.4(a) shows that the dislocation growth periods are 60 nm and 120 nm, and the periodic distances of dislocation growth are about 2 h and 4 h, respectively. When the growth period is 60 nm, 100 $In_{0.82}Ga_{0.18}As$ epitaxial layer lattices will correspond to 102 substrate lattices. The HRTEM image of the frame area in Fig.4(a) was detected and shown in Fig.4(b). There are 100 $In_{0.82}Ga_{0.18}As$ epitaxial layers in this period, which is the same as the above calculation result.

To obtain the carrier concentration of $In_xGa_{1-x}As$ epitaxial layer, the Hall effect measurement has been carried out on the samples A, B and C. According to the Hall effect principle, we have

$$n=\frac{1}{|R_H|q},\ \mu=\frac{1}{nq\rho}\ , \tag{6}$$

where n is the carrier concentration, R_H is Hall coefficient, μ is carrier mobility, ρ is resistivity, and q is electronic charge. It is known that the Hall coefficient R_H is inversely proportional to the carrier concentration n, and the carrier mobility μ is inversely proportional to the carrier concentration n. Tab.2 presents the Hall parameters of the samples and it is found that the carrier concentration in sample B with high In content is larger than that in sample A, and its carrier mobility is lower than that of sample A. The lowest carrier concentration is got from sample C.

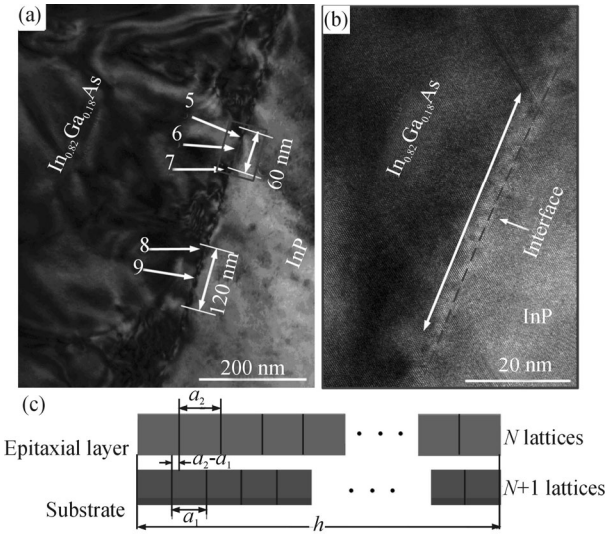

Fig.4 (a) Cross-sectional TEM image for the interface of $In_{0.82}Ga_{0.18}As$ epitaxial layer and InP substrate; (b) Corresponding HRTEM image around the interface; (c) Schematic of atomic arrangement at the interface

The dislocations are generated by the release of the mismatch stress in the growth process, which causes aggregation of the surface atoms, affects the surface structure of the epitaxial layer, and finally forms a relatively rough surface. At the same time, the atomic arrangement is distorted around the dislocation, resulting in large distortion energy, which can produce more point defects, so that the carrier concentration of sample B increases. The dislocation line has scattering effect on the carrier and the high dislocation density increases the scattering probability, so the carrier mobility decreases[23,24]. However, with the $In_{0.82}Ga_{0.18}As$ buffer layer, the misfit dislocations can be inhibited by the interface effectively. The dislocation density decreases obviously, so the carrier mobility increases.

Tab.2 Parameters of $In_xGa_{1-x}As$ epitaxial layers for samples A, B and C

Sample	Hall coefficient R_H ($\times 10^{-3}$ cm^3·C^{-1})	Carrier concentration n ($\times 10^{21}$ cm^{-3})	Carrier mobility μ ($\times 10^2$ cm^2·Ω^{-1})
A	1.898 0	3.318 95	1.113 8
B	1.450 8	4.399 90	0.883 9
C	22.878 9	0.283 86	25.548 0

The surface morphology, microstructure and the Hall coefficient of $In_xGa_{1-x}As$/InP heterostructure materials have been studied by HRTEM, SEM, AFM, Raman scattering spectroscopy and Hall effect measurements. The rough surface morphology, low Hall coefficient and high

carrier concentration are got in the high In content $In_xGa_{1-x}As/InP$ system. The $In_{0.82}Ga_{0.18}As$ buffer layer grown on the substrate favors the growth of the $In_{0.82}Ga_{0.18}As$ epitaxial layer because they match well with each other. In addition, due to the release of mismatch stress, misfit dislocations form with periodic arrangement. The minimum period has been calculated as 30 nm, consisting of 50 $In_{0.82}Ga_{0.18}As$ epitaxial layer lattices and 51 substrate lattices. The actual period in this paper is 60 nm or 120 nm, which is multiple of 30 nm. These results have a great guiding significance in analysis of the evolution and dislocation mechanism.

References

[1] X. Jin, H. Nakahara, K. Saitoh, T. Saka, T. Ujihara, N. Tanaka and Y. Takeda, Journal of Crystal Growth **353**, 84 (2012).

[2] M. Hostut, M. Alyoruk, T. Tansel, A. Kilic, R. Turan, A. Aydinli and Y. Ergun, Superlattices & Microstructures **79**, 116 (2015).

[3] N. Tounsi, M.M. Habchi, Z. Chine, A. Rebey and B. El Jani, Superlattices & Microstructures **59**, 133 (2013).

[4] S.H. Huynh, M.T.H. Ha, H.B. Do, Q.H. Luc and H.W. Yu, Applied Physics Letters **109**, 10 (2016).

[5] F. Zheng, C.Wang, Z. B. Sun and G.J. Zhai, Journal of Optoelectronics·Laser **25**, 1254 (2014). (in Chinese)

[6] S.J. Lin, J.J. Li, L.J. He, J. Den and J. Han, Journal of Optoelectronics·Laser **25**, 1471 (2014). (in Chinese)

[7] T. Mano, K. Mitsuishi, N. Ha, A. Ohtake and A. Castellano, Crystal Growth & Design **16**, 5412 (2016).

[8] J.L. Weyher, R. Fornari, T. Görög, J.J. Kelly and C.B. Erné, Journal of Crystal Growth **141**, 57 (1994).

[9] P.D. Casa, A. Maaßdorf, U. Zeimer and M. Weyers, Journal of Crystal Growth **434**, 116 (2016).

[10] J.G. Grabmaier and C.B. Watson, Physical Status Solidi **32**, K13 (1969).

[11] T. Takenaka, H. Hayashi, K. Murata and T. Inoguchi, Jpn J. Applied Physics Letters **17**, 1145 (1978).

[12] S. Emura, S. Gonda and Y. Matsui, Physical Review B **38**, 3280 (1988).

[13] M.R. Islam, P. Verma and M. Yamada, Jpn J. Applied Physics **41**, 991 (2002).

[14] J.P. Estrera, P.D. Stevens and R. Glosser, Applied Physics Letters **61**,1927 (1992).

[15] J. Groenen, G. Landa and R. Carles, J. Applied Physics **82**, 803 (1997).

[16] G. Burns, C.R. Wie and F.H. Dacol, Applied Physics Letters **51**, 1919 (1987).

[17] B. Jusserand, P. Voisin and M. Voos, Applied Physics Letters **46**, 678 (1985).

[18] F. Cerdeira, C.J. Buchenauer and F.H. Pollak, Physical Review B **5**, 580 (1972).

[19] R.J. Nicholas, L.C. Brunel and S. Huant, Physical Review Letter **55**, 883 (1985).

[20] T. Sasaki, A.G. Norman, M.J. Romero, M.M. Al-Jassim, M.Takahasi, N. Kojima, Y. Ohshita and M. Yamaguchi, Physical Status Solidi C **10**, 1640 (2013).

[21] J.P. Li, G.Q. Miao, Z.W. Zhang and Y.G. Zeng, Cryst. Eng. Comm. **17**, 5808 (2015).

[22] M. Fatemi and R.E. Stahlbush, Applied Physics Letters **58**, 825 (1991).

[23] Bai Y, Lee K E and Cheng C, J. Applied Physics **104**, 084518 (2008).

[24] Chen Y W, Hsu W C and Hsu R T, Solid-State Electronics **48**, 119 (2004).